Facile Synthesis of Macrocellular Mesoporous Foamlike Ce–Sn Mixed Oxides with a Nanocrystalline Framework by Using Triblock Copolymer as the Single Template

Le-Le Li, Jun Xu, Quan Yuan, Zhen-Xing Li, Wei-Guo Song, and Chun-Hua Yan*

Macrocellular mesoporous foamlike cerium–tin mixed oxide materials with well-defined porous structure and nanocrystalline frameworks are synthesized through a simple one-step self-assembly process using an amphiphilic triblock copolymer as the single template. The macrocellular pores are synthesized without the addition of any swelling agent or hazardous acids. The final mixed oxide possesses a hierarchically porous structure including macrocellular foam with ultralarge cell size, closed windows, and mesopores on the walls. This indicates that the porous structure can be notably stabilized and improved by the incorporation of Sn in the CeO_2. The materials are expected to be good candidates in catalysis, since the hierarchical porosity enables high surface areas and hence more chemically active sites associated with the mesopores, combined with the high efficiency of mass transport from the macrocellular foam. The catalytic characteristics are discussed in relation to the architectures of the materials, and it is revealed that the macrocellular/mesoporous materials would be an efficient catalyst for CO oxidation.

1. Introduction

Since mesoporous materials were first reported in 1992,[1] the interest in this research area has expanded all over the world due to wide applications in catalysis and other potential fields. Mesoporous materials are typically synthesized by self-assembly of the surfactant-type templates, among which amphiphilic block copolymers are valuable directing agents to obtain relatively large mesopores.[2,3] A representative example is two-dimensional hexagonal SBA-15 synthesized with triblock copolymer Pluronic P123 ($EO_{20}PO_{70}EO_{20}$; EO: ethylene oxide; PO: propylene oxide) as template.[2] Great efforts are focused on mesoporous materials with larger accessible pores. The commercially available PEO–PPO–PEO triblock copolymers themselves often lead to mesoporous silica with a pore size smaller than 20 nm.[3] Recently, colloidal templates have produced materials with larger spherical pores.[4] In contrast, these macroporous materials have much lower surface areas than the mesoporous materials. The synthesis of hierarchical structures possessing multiple scales of porosity has been achieved by the method of combining colloidal spheres and surfactants as dual templates.[5] However, the preparation of colloidal templates is either difficult or time-consuming.

Recently, siliceous mesocellular foam (MCF) materials, with spherical cells (>20 nm) three-dimensionally interconnected by windows,[6–11] have attracted much attention because of the facilitated access of the guest molecules to the internal surface of the mesostructure.[12–16] Generally, for the purpose

[*] Prof. C.-H. Yan, L.-L. Li, J. Xu, Dr. Q. Yuan, Z.-X. Li
Beijing National Laboratory for Molecular Sciences
State Key Laboratory of Rare Earth Materials Chemistry and
Applications
Peking University
Beijing 100871 (P. R. China)
E-mail: yan@pku.edu.cn

Prof. W.-G. Song
Beijing National Laboratory for Molecular Sciences
Institute of Chemistry, Chinese Academy of Sciences (CAS)
Beijing 100080 (P. R. China)

🖳 Supporting Information is available on the WWW under http://www.small-journal.com or from the author.

of expanding the pore diameter and synthesis of MCF materials, swelling agents such as trimethylbenzene, which dissolves in the more hydrophobic core of the liquid-crystalline template, are usually used.[6–11] Such a method is complex and sensitive to various synthetic parameters, such as the mixing conditions and the effect of pH and temperature.[6–11] Recently, the preparation of MCF materials without the use of swelling agents has been reported.[17–20] Kim, Hyeon, and co-workers reported a simple and cost-effective synthesis of a siliceous MCF material with ordered mesoporous walls by using an amphiphilic triblock copolymer as structure-directing agent.[17] With the aid of NaCl and alcohol, siliceous MCF was also successfully synthesized by using an amphiphilic triblock copolymer as template.[18] Yang et al. explored the swelling-agent-free synthesis of MCF-like silica mesophases by a pH-dependent structural transformation using special carboxy-terminated triblock copolymer Pluronic P123 as template.[19] However, to date the successful synthesis of MCF has been mainly limited to silicate components primarily due to the ease of controlling the hydrolysis and polycondensation of silicon alkoxides.[6–20] Compared to porous silica, porous metal oxides have much more potential for applications in catalysis, solar cells, sensors, and electrode materials because of their intrinsic properties.[21] Furthermore, this potential can be maximized in porous metal oxides with highly crystalline walls.[21–26] Fabrication of MCF-like metal oxides with a crystalline framework through a simple and economic approach remains a particular challenge.

Within the huge family of binary and ternary metal oxides, ceria (CeO_2) has been the subject of numerous investigations in recent years and excellent reviews are available that discuss different aspects, from the structural properties to their wide applications in catalysis, electrochemistry, and optics.[27] For instance, CeO_2-based materials have important applications as promoters of three-way catalysts (TWCs) to reduce the emission of toxic pollutants from automobile exhaust, due to their high oxygen-storage capacity (OSC), rich oxygen vacancies, and low redox potential between Ce^{3+} and Ce^{4+}.[27,28] For many such applications, it is highly desirable to prepare mesoporous crystalline CeO_2 systems.[29,31–35] However, the synthesis of thermally stable mesoporous CeO_2 represents a much more complex problem due to its susceptibility to hydrolysis as well as the breakdown of the mesostructure upon the final crystallization step.[29] Recently, Antonietti et al. developed a new type of block copolymer of the KLE family (poly(ethylene-co-butylene)-block-poly(ethylene oxide)), which has enabled the synthesis of various metal oxide thin films with pronounced crystallinity and good mesostructural order.[30,31] By taking advantage of this novel block copolymer as template, for the first time mesoporous ceria film with a homogeneous pore size of about 10 nm and highly crystalline walls was obtained by evaporation-induced self-assembly.[31] Nanocrystalline mesoporous CeO_2 was also achieved by a more laborious nanocasting process (with mesoporous silica or carbon as the hard template)[32] or by assembly of crystalline CeO_2 nanoparticles in the presence of structure-directing agents.[33]

Although various studies have been devoted to the preparation of CeO_2 with one type of mesopore, very few

efforts have focused on the fabrication of a hierarchically porous structure with multiscaled porosity.[35] In general, such multiscaled pore systems have obvious advantages and are more suitable for most potential applications in terms of diffusion efficiency and accessibility to the pores by guest species.[5] Most recently, a major leap in the preparation of hierarchically porous CeO_2 film with a highly crystalline framework and a bimodal pore size distribution has been achieved by Smarsly et al.[35] In this route, the use of suitable co-templates, the KLE block copolymer and an ionic liquid, resulted in a system of deformed spherical mesopores of size about 6×16 nm^2 with wormlike pores about 2.5–3.0 nm in diameter between them. The stabilization of hierarchically porous CeO_2 materials by a one-step, convenient, and economic approach would be a breakthrough in the catalysis field, in which ordered porosity, high surface area, excellent mass transport, and good crystallinity are simultaneously required.

Herein, a macrocellular mesoporous foamlike cerium–tin mixed oxide with well-defined porous structure and nanocrystalline framework was synthesized through a simple one-step self-assembly process using the amphiphilic triblock copolymer Pluronic F127 ($EO_{106}PO_{70}EO_{106}$) as the single template. In this method, the macrocellular pores are synthesized without adding any swelling agent or hazardous acids. Interestingly, the final mixed oxide is a hierarchically porous structure possessing macrocellular foam with ultralarge cell size, closed windows, and mesopores on the walls. This indicates that the porous structure can be notably stabilized by the introduction of Sn into the CeO_2. As a possible application, the catalytic activity of the material for CO conversion is examined and discussed in relation to the architecture of the material.

2. Results and Discussion

2.1. Structural Characteristics

It is well known that pure ceria has poor thermal stability and undergoes rapid sintering under high-temperature conditions.[27] An alternative way to overcome this problem is the substitution of other transition- and non-transition-metal ions (Zr^{4+}, Ti^{4+}, Sn^{4+}, etc.) into the original ceria cubic structure to form mixed oxides, which offers the opportunity to avoid the otherwise excessive grain growth and to improve the thermal stability and performance of the materials.[27,34,36] Our results demonstrate that the cross-doping of Sn within the CeO_2 is a key to the successful organization of the macrocellular mesoporous foamlike structure. No hierarchically porous structure is obtained when other metal ions are used as dopants with this synthetic method.
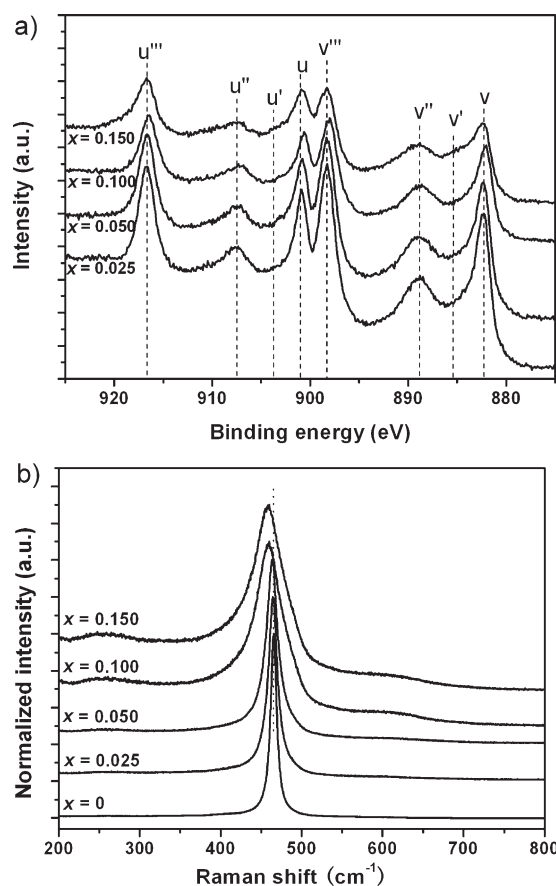
Figure 1a shows the powder X-ray diffraction (PXRD) patterns of cerium–tin mixed oxides with different Sn contents x ($x = 0.025$–0.150) calcined at 400 °C. All the diffraction peaks for each sample can be indexed to (111), (200), (220), (311), (322), and (400) reflections, which correspond to a face-centered cubic (fcc) fluorite structure. An X-ray fluorescence (XRF) instrument was utilized to check the metal compositions of the as-prepared products (Table S1 in the Supporting Information), and the results show that the experimental
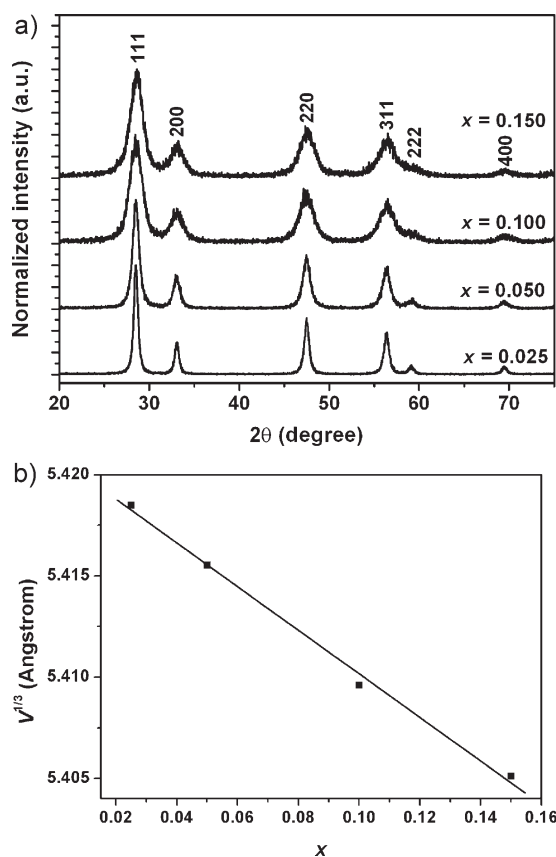
Figure 1. a) XRD patterns of $Ce_{1-x}Sn_xO_2$ ($x = 0.025-0.150$) calcined at 400 °C. b) Cube root of the lattice volume ($V^{1/3}$) of the $Ce_{1-x}Sn_xO_2$ samples calcined at 400 °C as a function of SnO_2 content x.

Figure 2. a) XPS Ce 3d spectra of the as-prepared $Ce_{1-x}Sn_xO_2$ samples. b) Raman spectra of the $Ce_{1-x}Sn_xO_2$ ($x = 0-0.150$) samples.

contents of Ce and Sn were in good agreement with the target ones. With an increase of Sn content, the XRD peaks gradually shift to higher diffraction angles. Figure 1b displays the nearly linear relationship between the cube root of lattice volume ($V^{1/3}$) and the tin content x of the $Ce_{1-x}Sn_xO_2$ sample. According to Vegard's law, the studied cerium–tin mixed oxides can be assigned to solid solutions.[36] This reveals that the smaller Sn^{4+} ion can substitute the position of the Ce^{4+} ion in the doping range of $x = 0.025-0.150$ in the present synthetic method. When $x > 0.15$, the typical SnO_2 phase, tetragonal-structure features appear in the PXRD pattern (Figure S1 in the Supporting Information), which evinces the heterogeneous phase separation that forms both CeO_2 and SnO_2. The crystal sizes of the solid solution estimated from the (111) peaks were 15.8, 9.6, 4.6, and 4.5 nm for the $Ce_{1-x}Sn_xO_2$ samples with $x = 0.025, 0.050, 0.100,$ and 0.150, respectively, which agreed well with the results observed with transmission electron microscopy (TEM) as described later. Therefore, in comparison with the undoped CeO_2 sample, the proper introduction of Sn and thus the formation of a solid solution inhibited crystalline grain growth by providing dissimilar boundaries.[27,36] The broadening of the peaks confirmed that the $Ce_{1-x}Sn_xO_2$ composites were composed of primary small particles.

As UV blocking and shielding materials, CeO_2 nanomaterials can exhibit strong absorption capability in the ultraviolet range. For pure CeO_2, there is a strong absorption band below

400 nm as shown in the UV/Vis spectra (Figure S2 in the Supporting Information), which is due to the charge-transfer transition from O^{2-} (2p) to Ce^{4+} (4f) orbitals in CeO_2.[37] The absorption spectra of Sn^{4+}-doped CeO_2 nanostructures exhibit a blue shift compared with pure CeO_2. For CeO_2 nanocrystals, it is well known that a small amount of Ce^{3+} coexists at the surface of CeO_2, which increases with decreasing particle size.[38] The presence of Ce^{3+} ions in the Ce−Sn mixed oxide can also be confirmed by X-ray photoelectron spectroscopy (XPS) analysis, as shown in Figure 2a. The complex spectrum of Ce 3d can be decomposed into eight components with the assignment defined in Figure 2a. It can be seen that the chemical valence of cerium was mainly Ce^{4+} plus a small fraction of Ce^{3+}. The relative intensities of v' and u' to the other six bands increased with increasing Sn content x, thus revealing that the Ce^{3+} to Ce^{4+} ratio of the as-prepared $Ce_{1-x}Sn_xO_2$ materials was enhanced by the incorporation of Sn. Due to the change from Ce^{4+} to Ce^{3+} ions, the charge-transfer gap between O 2p and Ce 4f bonds increased, which led to the blue shift in the absorption spectrum for Ce−Sn mixed oxides compared with bulk CeO_2.[39]

Figure 2b shows typical Raman spectra of the $Ce_{1-x}Sn_xO_2$ composites. For pure CeO_2, there is an obvious band at 465 cm^{-1}, the band of a fluorite structural material, which is assigned to F_{2g} symmetry as a symmetric breathing mode of the oxygen atoms around the cerium ions.[40] It can be seen that,
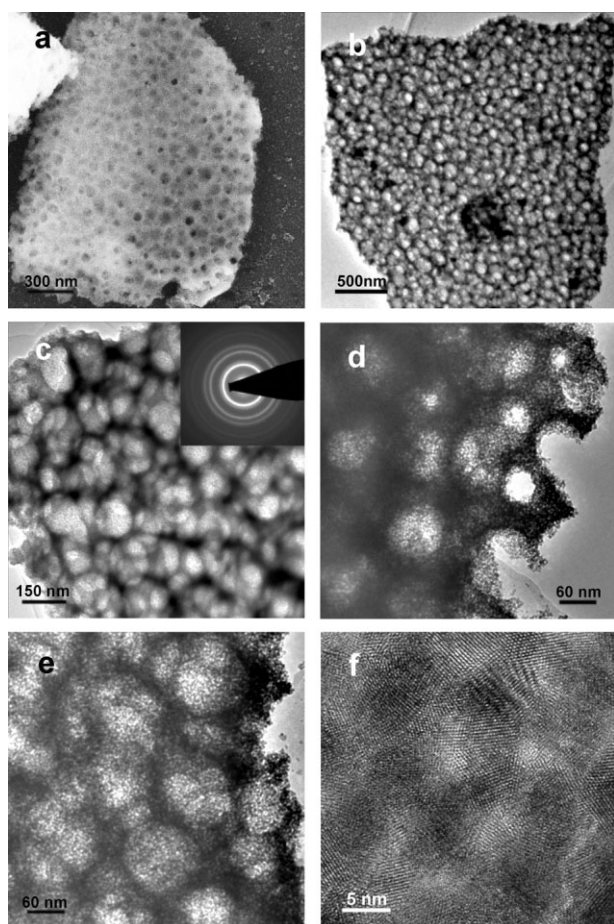
Figure 3. a) Representative SEM image, b,c) typical TEM images, and d–f) high-magnification TEM images of the hierarchically macrocellular/mesoporous $Ce_{0.9}Sn_{0.1}O_2$ materials calcined at 400 °C. The inset in (c) is the corresponding SAED pattern.

with the increase of Sn content, there is a small systematic shift of the bands at $465\ cm^{-1}$ to lower frequencies, which is due to the fact that the insertion of Sn ions decreases the vibration frequency of the metal–anion band and the change of the lattice parameter. This also indicates that the incorporation of Sn into the ceria lattice results in the formation of a solid solution, which is in agreement with the results deduced from XRD analysis. In addition, it is important to notice that a new Raman band is observed at $600\ cm^{-1}$ with an increase of Sn content in the $Ce_{1-x}Sn_xO_2$ solid solution. It is known that this band results from lattice defects and the formation of oxygen vacancies, so that the material can absorb and give off oxygen easily and enhances OSC, which is especially important to improve the activity of the oxygen ions for catalytic reactions.[40]

Figure 3 shows the representative scanning electron microscopy (SEM) and TEM images of the $Ce_{0.9}Sn_{0.1}O_2$ composite calcined at 400 °C. It can be seen that the material exhibits a foamlike morphology and a three-dimensional (3D) macrocellular network structure with ultralarge cell diameter in the range 60–150 nm, which indicates a homogeneous macrocellular foam structure (Figure 3a–c). The cells are connected by comparatively narrow windows of size 20–50 nm. Figure 3d and e show typical TEM images of the prepared sample, in

which uniformly distributed wormhole-like mesopores on the macrocellular walls are clearly observed. Also, small-angle X-ray scattering (SAXS) of the sample (Figure S3 in the Supporting Information) shows a broader primary peak with a corresponding d_{100} distance of about 8.5 nm, which further confirms a short-range-ordered pore network. No reflection peak is detected for the $Ce_{1-x}Sn_xO_2$ samples with $x < 0.10$, which demonstrates the importance of the incorporation of tin for the formation of the mesostructure. The high-resolution TEM image (Figure 3f) shows nanocrystallites with well-defined lattice planes, thus demonstrating the high crystallinity of the pore walls, which was also confirmed by selected-area electron diffraction (SAED; inset of Figure 3c). The crystallites are randomly oriented, as seen from the lattice fringes. Furthermore, the scanning transmission electron microscopy–X-ray energy-dispersive spectroscopy (STEM-EDS) characterization (Figure S4 in the Supporting Information), which was used to investigate the elemental compositions of the materials in the microdomain, also confirms the 9:1 molar ratio between Ce and Sn, thus indicating the good stoichiometric homogeneity of the $Ce_{0.9}Sn_{0.1}O_2$ product. TEM investigations (Figure S5 in the Supporting Information) also confirm that the macrocellular mesoporous foam is retained even after treatment at 600 °C, which suggests the higher thermal stability of the materials.

The structure of the $Ce_xSn_{1-x}O_2$ composites with different Ce/Sn ratios that were calcined at 400 °C was also analyzed by TEM measurement (Figure S6 in the Supporting Information). No porous structure was observed for the pure CeO_2. However, with the introduction of Sn and the formation of a solid solution, a macrocellular mesoporous foam was gradually observed for the composites. In general, crystalline mesoporous oxides possessing both nanopores and crystalline walls are desirable for many applications. Yet it is often the case that higher-temperature treatment results in transformation of the material to the crystalline state and a subsequent loss of the mesostructure.[22–26,29] Thus, it is reasonable to deduce that the hierarchically porous structure for this CeO_2-based composite can be significantly stabilized and improved by the incorporation of Sn due to the inhibition of crystalline grain growth,[27,36] which is in agreement with the XRD results.

The macrocellular foam materials possess a narrow distribution of mesopores on the macrocells, as further evidenced by nitrogen adsorption measurements. Figure 4 shows nitrogen adsorption–desorption isotherms and the corresponding pore size distribution of the $Ce_{0.9}Sn_{0.1}O_2$ samples calcined at 400 °C. The crystalline materials exhibit typical type IV isotherms with a distinct condensation step at a P/P_0 range of 0.5–0.8, which signifies the mesoporous structure. The presence of a pronounced hysteresis loop in the isotherm curve is indicative of the pores in a 3D intersection network. A high Brunauer–Emmett–Teller (BET) surface area of $124\ m^2\ g^{-1}$ and a total pore volume of $0.26\ cm^3\ g^{-1}$ can be obtained for the nanocrystalline $Ce_{0.9}Sn_{0.1}O_2$ materials. Barrett–Joyner–Halenda (BJH) calculations derived from desorption data reveal a narrow pore size distribution centered at 3.5 nm. The nitrogen adsorption–desorption analysis of the $Ce_{1-x}Sn_xO_2$ samples (Figure S7 and Table S2 in the Supporting Information) indicates that the BET surface areas increase greatly with the increase of the Sn/Ce ratios, further confirming
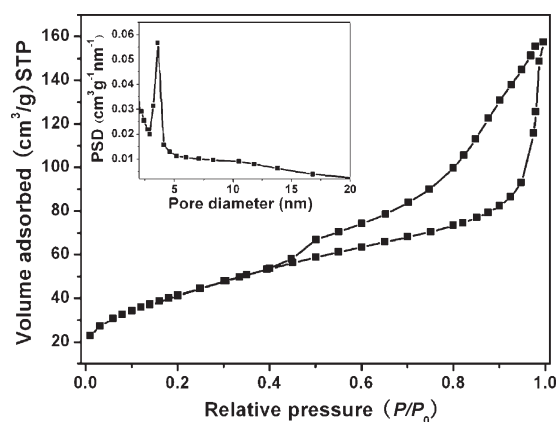
Figure 4. Nitrogen adsorption–desorption isotherm and (inset) the corresponding pore size distribution of the hierarchically porous $Ce_{0.9}Sn_{0.1}O_2$ material calcined at 400 °C.

that the porous structure can be notably improved by the incorporation of Sn in the composites, which agrees well with the above TEM results. The large surface area and bimodal porous structure combined with the excellent thermal stability enhance the potential applications of these macrocellular/mesoporous foamlike cerium–tin mixed oxides in catalysis.

According to the above SEM and TEM observations and BET analysis, it can be seen that the macrocellular mesoporous foamlike structure of cerium–tin mixed oxide with a nanocrystalline framework can be easily prepared through a simple sol–gel route with triblock copolymer F127 as the single template. This suggests a cooperative self-assembly mechanism in which the block copolymer acts as a twofold templating agent, which not only directs the process among Ce and Sn species and the formation of the mesophase, but also templates the aggregation of the mesostructure by the formation of vesicles (otherwise known as supermicelles).[41] The MCF-like material is then obtained through template removal, and resembles spherical macrocellular cells interconnected by windows with mesopores on the walls (Figure 5). This mechanism is most likely related to that proposed for macro/mesoporous zirconia[42] and mesocellular mesoporous silica,[17] which were also prepared with a single surfactant as template. Through a similar pathway, small-sized mesostructure building blocks with wormlike pores templated by P127 are initially formed, and then large vesicle-type micelles are responsible for the formation of the macrocellular pores.[17] The factors that influence the formation of the hierarchically porous structures were studied, and it was found that 40 °C and 50% relative humidity (RH) are the optimum conditions in the present work, which are controllable and repeatable for the organization of hierarchically porous composite structures.

It is worth highlighting the simple swelling-agent-free synthesis of MCF-like functional metal oxides. Furthermore, in most cases, to fabricate mesoporous metal oxides, hazardous acids are often necessary to slow down the hydrolysis–condensation rate of the metal precursors and to avoid undesirable phase separation.[21–26] Herein, no extra acid is added in this procedure; however, the hydrolysis of ceric nitrate and tin chloride is a synchronized and self-adjusted process,
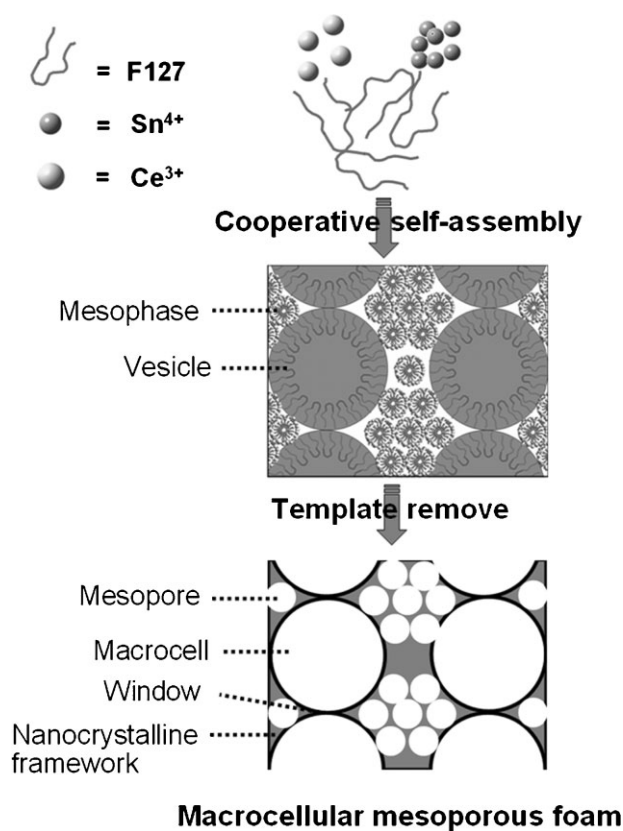

Figure 5. Possible mechanistic scheme for the formation of the hierarchically macrocellular/mesoporous foamlike cerium–tin mixed oxide with nanocrystalline framework by using a triblock copolymer as single template.

which results in a homogeneous framework with good dispersion of these two metal species. Our synthesis strategy is a bit similar to the acid–base pair approach proposed for mesoporous minerals, such as the MPO system, by Zhao et al.[43] Although the formation mechanism of MCF-like structures has been proposed, the more detailed aspects of the formation of these novel materials need further investigation.

2.2. Catalytic Performance

To test the surface acidity of $Ce_{1-x}Sn_xO_2$ composites with different Ce/Sn ratios that were calcined at 400 °C, Fourier transform infrared (FTIR) pyridine adsorption measurements were performed. As shown in Figure 6, the IR spectra of adsorbed pyridine display characteristic absorption bands at 1620 and 1450 cm^{-1} corresponding to the ν_{8a} and ν_{19b} modes of the ring-breathing vibrations $\nu(CCN)$ of pyridine, respectively, which indicate pyridine adsorption on Lewis acid sites.[44] The amount of adsorbed pyridine on such sites is estimated by integration of the absorbance band (ν_{19b} mode) around 1450 cm^{-1}. The relative numbers of Lewis acid sites calculated for $Ce_{1-x}Sn_xO_2$ are increased greatly with the introduction of Sn (Table S3 in the Supporting Information), which can be attributed to the increased surface-to-volume ratios associated with the formation of hierarchically porous structures. Strong Lewis acidity proves that these hierarchically structured
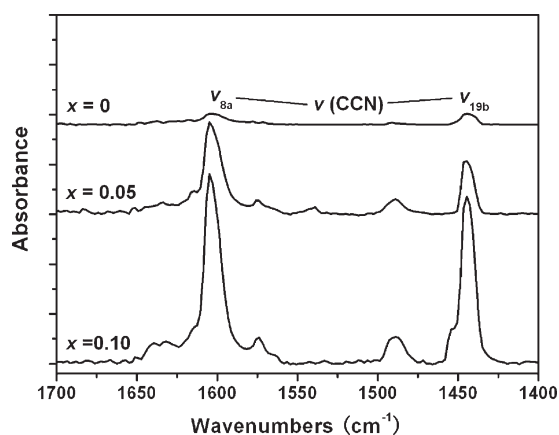
Figure 6. FTIR spectra of pyridine adsorption for the materials $Ce_{1-x}Sn_xO_2$ ($x = 0$–0.10) at a deposition temperature of $200\,°C$.

cerium–tin mixed oxides with bimodal pore distribution on the meso- and macroscale should be ideal supports for heterogeneous catalysis.[45]

The elimination of CO is of fundamental importance in automotive pollution control, fuel cells, and many other applications.[28] The steady-state conversion of carbon monoxide to carbon dioxide using the obtained materials was measured and is shown in Figure 7. The CO conversion increased with increasing reaction temperature for all the samples, and the as-obtained $Ce_{0.9}Sn_{0.1}O_2$ with MCF-like structure (denoted hereinafter as macro-/meso-$Ce_{0.9}Sn_{0.1}O_2$) shows a much better performance for CO removal than the pure CeO_2 particles prepared by the same procedure. This could be assigned to the interactions between CeO_2 and the dopant oxide SnO_2 and the formation of solid-solution materials, which exhibit improved thermal stability, controlled porous structure, and high specific surface area. The macrocellular mesoporous $Ce_{0.9}Sn_{0.1}O_2$ has proven to be an ideal catalyst support. Loaded with $0.8\,wt\%$ of 2.6-nm Pt nanoparticles, the Pt/macro-/meso-$Ce_{0.9}Sn_{0.1}O_2$ catalyst showed a much higher catalytic activity than macro-/meso-$Ce_{0.9}Sn_{0.1}O_2$. A 100% CO conversion was achieved at $150\,°C$ for Pt/macro-/meso-$Ce_{0.9}Sn_{0.1}O_2$, while it
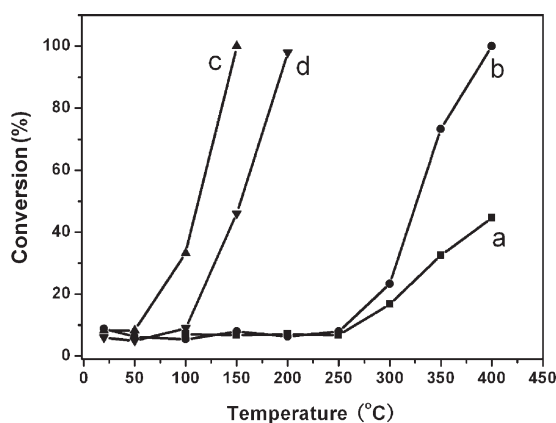
Figure 7. CO conversion as a function of temperature for the as-prepared CeO_2 (line a), hierarchical macrocellular/mesoporous $Ce_{0.9}Sn_{0.1}O_2$ (line b), Pt/macro-/meso-$Ce_{0.9}Sn_{0.1}O_2$ catalyst (line c), and Pt/meso-$Ce_{0.9}Sn_{0.1}O_2$ catalyst (line d).

needed $400\,°C$ for total conversion with pure macro-/meso-$Ce_{0.9}Sn_{0.1}O_2$. Also, the half CO conversion temperatures for both samples were 110 and $330\,°C$, respectively. Obviously, the load of Pt nanoparticles significantly increased the catalytic activity of $Ce_{0.9}Sn_{0.1}O_2$ materials. This could be attributed to the strong synergistic interaction between the noble metal Pt and $Ce_{0.9}Sn_{0.1}O_2$.[28] $Ce_{0.9}Sn_{0.1}O_2$ supplied reactive oxygen by releasing/taking up oxygen through a redox process involving the Ce^{4+}/Ce^{3+} couple. During the catalytic CO oxidation process, reactive oxygen from the support reacted with CO molecules adsorbed on Pt nanoparticles to form CO_2.[28] These results imply that the synthesized Pt/macro-/meso-$Ce_{0.9}Sn_{0.1}O_2$ catalyst has a high potential in future applications involving CO oxidation in which a low-temperature working environment is desired.

To further confirm the positive effects of the macrocellular foamlike structure on catalytic activity, mesoporous $Ce_{0.9}Sn_{0.1}O_2$ without the macrocellular feature was prepared by using Brij 56 ($C_{16}EO_{10}$) as structure-directing agent. The XRD pattern of the obtained meso-$Ce_{0.9}Sn_{0.1}O_2$ calcined at $400\,°C$ indicates an fcc fluorite structure with a crystal size of $4.7\,nm$. TEM images further confirm that the sample has a wormlike mesoporous structure without macrocells. Nitrogen sorption measurements show a BET surface area of $117\,m^2\,g^{-1}$ and a narrower pore size distribution of $3.5\,nm$. All these characteristics (Figure S8 in the Supporting Information) indicate that the obtained meso-$Ce_{0.9}Sn_{0.1}O_2$ has almost the same phase structure, grain size, BET surface area, and mesopore size as the macro-/meso-$Ce_{0.9}Sn_{0.1}O_2$. This can provide an effective means to examine the influence of the macrocellular foam feature on catalytic properties. Loaded with the same content ($0.8\,wt\%$) of 2.6-nm Pt nanoparticles, the Pt/meso-$Ce_{0.9}Sn_{0.1}O_2$ catalyst was employed for the oxidation of CO (Figure 7). A 100% CO conversion was achieved at about $200\,°C$ for Pt/meso-$Ce_{0.9}Sn_{0.1}O_2$, $50\,°C$ higher than for the Pt/macro-/meso-$Ce_{0.9}Sn_{0.1}O_2$. This can be understood by considering the decreased mass-transfer resistance provided by the interconnected macrocells that persist throughout the support. Hierarchically porous structures not only can provide potentially high surface areas, but also can process reactant molecules efficiently with fast diffusion to the active sites within the mesopores.[35] Bimodal as well as fractal pore structures have been investigated theoretically for diffusion-limited processes, and were found to increase catalytic efficiency effectively.[46] Thus, an efficient catalyst could be a hierarchically porous structure that combines large cells (enabling high molecular diffusion rates and mass transport efficiency) with smaller pores (ensuring high surface areas and chemically active sites) in a 3D connected network.[47]

3. Conclusions

Macrocellular mesoporous foamlike cerium–tin mixed oxides with a nanocrystalline framework have been synthesized through a simple one-step process involving triblock copolymer as a single template. In this synthesis, the macrocellular pores are obtained without adding any swelling agent or hazardous acids. The final mixed oxide is a hierarchically porous structure

including macrocellular foam with ultralarge cell size and mesopores on the walls. The obtained multimetallic materials exhibit high thermal stability, possess high surface areas and large numbers of surface Lewis acid sites, and show interesting catalytic activities for CO conversion. The catalytic characteristics were discussed in relation to the architectures of the materials, which disclose that the hierarchically macrocellular/mesoporous materials would be better catalysts. This hierarchically structured cerium–tin mixed oxide with bimodal pore distribution on the meso- and macroscale should find further applications in various catalysis and purification processes. Furthermore, the interpenetrating bimodal pores, nanocrystalline networks, and good particle/particle junctions make this nanomaterial of interest in solid oxide fuel cell applications.[24,48]

4. Experimental Section

Synthesis method: Pluronic F127 (0.9 g) was dissolved in ethanol (10 mL) at room temperature. Then quantitative amounts of $Ce(NO_3)_3 \cdot 6H_2O$ and $SnCl_4 \cdot 5H_2O$ (total Ce plus Sn was 5 mmol) were added to the above solution with vigorous stirring. The mixture was stirred for 12 h at room temperature while sealed with polyethylene film. After 2 days of solvent evaporation at 40 °C and RH 50%, the gel product was dried in an oven at 60 °C for 2 days and then at 100 °C for 1 day. Calcination was carried out by slowly increasing the temperature from room temperature to 400 °C (1 °C min^{-1} ramping rate) and heating at 400 °C for 3 h in air. Mesoporous $Ce_{0.9}Sn_{0.1}O_2$ without macrocells was prepared through the same procedure by using Brij 56 (0.6 g) instead of Pluronic F127 as structure-directing agent.

Catalyst preparation: Platinum particles were synthesized according to literature methods.[49] Pt colloidal aqueous solution (10 mL, 12 mM) was mixed with ethanol (10 mL). The mixture was quickly added to macro-/mesoporous $Ce_{0.9}Sn_{0.1}O_2$ (0.4 g) and, for comparison, mesoporous $Ce_{0.9}Sn_{0.1}O_2$ (denoted as Pt/macro-/meso-$Ce_{0.9}Sn_{0.1}O_2$ and Pt/meso-$Ce_{0.9}Sn_{0.1}O_2$, respectively), and the slurry was sonicated for 3 h at room temperature. The precipitates were separated by centrifugation, washed with water and ethanol, dried in an oven at 100 °C, and then calcined at 300 °C for 3.5 h in air.

Characterization: PXRD patterns were recorded on a Rigaku (Japan) DMAX-2000 diffractometer using CuKα ($\lambda = 1.5405$ Å) radiation. XRF data were obtained from a Bruker S4 Explorer spectrometer at a power of 1 kW. XPS measurements were carried out in the ion-pumped chamber (evacuated to 2×10^{-9} Torr) of an Escalad 5 (UK) spectrometer employing MgKα radiation (binding energy BE = 1253.6 eV). Laser Raman spectra were recorded on a Jobin-Yvon HR800 Raman spectrometer with a 12-mW He−Ne laser (632.8 nm). SAXS measurements were performed with a high-flux instrument (SAXSess, Anton Paar) employing CuKα radiation at room temperature. SEM observations were carried out with a DB-235 focused ion-beam (FIB) system operated at an acceleration voltage of 15 kV. TEM and energy-dispersive X-ray analysis (EDAX) were performed on a Hitachi H-9000 NAR transmission electron microscope (Japan) under a working voltage of 300 kV. The nitrogen adsorption–desorption isotherms at 78.3 K were measured by using an ASAP 2010 analyzer (Micromeritics Co. Ltd., USA). The Pt content of the catalyst was determined on an inductively coupled plasma–atomic emission spectrometer (Vista, Varian).

CO oxidation test: A homemade flow reactor system including a quartz reaction tube (8×42 mm^2) was used for the catalytic test. In a typical CO oxidation experiment, sample (50 mg) and sea sand (450 mg) were mixed as catalyst, and the experiment was carried out at a 25 SCCM flow of 1% CO in nitrogen and 25 SCCM air. The gas composition was monitored online on a Shimadzu GC-14C gas chromatograph equipped with a thermal conductivity detector.

[1] a) C. T. Kresge, M. E. Leonowicz, W. J. Roth, J. C. Vartuli, J. S. Beck, *Nature* **1992**, *359*, 710; b) J. S. Beck, J. C. Vartuli, W. J. Roth, M. E. Leonowicz, C. T. Kresge, K. D. Schmitt, C. T.-W. Chu, D. H. Olson, E. W. Sheppard, S. B. McCullen, J. B. Higgins, J. L. Schlenkert, *J. Am. Chem. Soc.* **1992**, *114*, 10834.
[2] a) D. Zhao, J. Feng, Q. Huo, N. Melosh, G. H. Fredrickson, B. F. Chmelka, G. D. Stucky, *Science* **1998**, *279*, 548; b) D. Zhao, Q. Huo, J. Feng, B. F. Chmelka, G. D. Stucky, *J. Am. Chem. Soc.* **1998**, *120*, 6024.
[3] a) Y. Wan, Y. Shi, D. Zhao, *Chem. Commun.* **2007**, 897; b) Y. Wan, D. Zhao, *Chem. Rev.* **2007**, *107*, 2821.
[4] a) B. T. Holland, C. F. Blanford, A. Stein, *Science* **1998**, *281*, 538; b) O. D. Velev, T. A. Jede, R. F. Lobo, A. M. Lenhoff, *Nature* **1997**, *389*, 447.
[5] a) P. D. Yang, T. Deng, D. Zhao, P. Feng, D. Pine, B. F. Chmelka, G. M. Whitesides, G. D. Stucky, *Science* **1998**, *282*, 2244; b) M. Antonietti, B. Berton, C. Göltner, H. Hentze, *Adv. Mater.* **1998**, *10*, 154; c) Y. Zhou, M. Antonietti, *Chem. Commun.* **2003**, 2564; d) D. Kuang, T. Brezesinski, B. Smarsly, *J. Am. Chem. Soc.* **2004**, *126*, 10534.
[6] P. Schmidt-Winkel, W. W. Lukens, D. Zhao, P. D. Yang, B. F. Chmelka, G. D. Stucky, *J. Am. Chem. Soc.* **1999**, *121*, 254.
[7] J. S. Lettow, Y. J. Han, P. Schmidt-Winkel, P. D. Yang, D. Zhao, G. D. Stucky, J. Y. Ying, *Langmuir* **2000**, *16*, 8291.
[8] P. Schmidt-Winkel, W. W. Lukens, P. D. Yang, D. I. Margolese, J. S. Lettow, J. Y. Ying, G. D. Stucky, *Chem. Mater.* **2000**, *12*, 686.
[9] W. W. Lukens, P. D. Yang, G. D. Stucky, *Chem. Mater.* **2001**, *13*, 28.
[10] S. S. Kim, T. R. Pauly, T. J. Pinnavaia, *Chem. Commun.* **2000**, 1661.
[11] A. Karkamkar, S. S. Kim, T. J. Pinnavaia, *Chem. Mater.* **2003**, *15*, 11.
[12] J. Kim, J. Lee, H. B. Na, B. C. Kim, J. K. Youn, J. H. Kwak, K. Moon, E. Lee, J. Kim, J. Park, A. Dohnalkova, H. G. Park, M. B. Gu, H. N. Chang, J. W. Grate, T. Hyeon, *Small* **2005**, *1*, 1203.
[13] S. Seelan, A. K. Sinha, K. Kato, Y. Yokogawa, *Adv. Mater.* **2006**, *18*, 3001.
[14] J. Shah, T. J. Pinnavaia, *Chem. Mater.* **2005**, *17*, 947.
[15] I. Park, T. J. Pinnavaia, *Adv. Funct. Mater.* **2007**, *17*, 2835.
[16] J. Liu, Q. Yang, L. Zhang, D. Jiang, X. Shi, J. Yang, H. Zhong, C. Li, *Adv. Funct. Mater.* **2007**, *17*, 569.

[17] J. Lee, J. Kim, J. Kim, H. Jia, M. Kim, J. H. Kwak, S. Jin, A. Dohnalkova, H. G. Park, H. N. Chang, P. Wang, J. W. Grate, T. Hyeon, *Small* **2005**, *1*, 744.

[18] S. Y. Chen, S. Cheng, *Chem. Mater.* **2007**, *19*, 3041.

[19] Y.-C. Hsu, Y.-H. Chang, C.-M. Yang, *Adv. Funct. Mater.* **2008**, *18*, 1799.

[20] H. Wang, Y. Wang, X. Zhou, L. Zhou, J. Tang, J. Lei, C. Yu, *Adv. Funct. Mater.* **2007**, *17*, 613.

[21] a) P. D. Yang, D. Y. Zhao, D. I. Margolese, B. F. Chmelka, G. D. Stucky, *Nature* **1998**, *396*, 152; b) D. Li, H. Zhou, I. Honma, *Nat. Mater.* **2004**, *3*, 65; c) J. Lee, M. C. Orilall, S. C. Warren, M. Kamperman, F. J. Disalvo, U. Wiesner, *Nat. Mater.* **2008**, *7*, 222; d) C.-K. Tsung, J. Fan, N. Zheng, Q. Shi, A. J. Forman, J. Wang, G. D. Stucky, *Angew. Chem.* **2008**, *120*, 8810; *Angew. Chem. Int. Ed.* **2008**, *47*, 8682.

[22] a) F. Schüth, *Angew. Chem.* **2003**, *115*, 3730; *Angew. Chem. Int. Ed.* **2003**, *42*, 3604; b) A.-H. Lu, F. Schüth, *Adv. Mater.* **2006**, *18*, 1793.

[23] M. Antonietti, G. A. Ozin, *Chem. Eur. J.* **2004**, *10*, 28.

[24] B. Smarsly, M. Antonietti, *Eur. J. Inorg. Chem.* **2006**, 1111.

[25] Y. Wan, H. F. Yang, D. Y. Zhao, *Acc. Chem. Res.* **2006**, *39*, 423.

[26] S. W. Boettcher, J. Fan, C. K. Tsung, Q. Shi, G. D. Stucky, *Acc. Chem. Res.* **2007**, *40*, 784.

[27] a) J. Kašpar, P. Fornasiero, M. Graziani, *Catal. Today* **1999**, *50*, 285; b) J. Kašpar, P. Fornasiero, N. Hickey, *Catal. Today* **2003**, *77*, 419.

[28] a) S. Carrettin, P. Concepción, A. Corma, J. M. L. Nieto, V. F. Puntes, *Angew. Chem.* **2004**, *116*, 2592; *Angew. Chem. Int. Ed.* **2004**, *43*, 2538; b) P. Concepción, A. Corma, J. Silvestre-Albero, V. Franco, J. Y. Chane-Ching, *J. Am. Chem. Soc.* **2004**, *126*, 5523.

[29] a) M. Lundberg, B. Skarman, F. Cesar, L. Reine Wallenberg, *Micropor. Mesopor. Mater.* **2002**, *54*, 97; b) D. Terribile, A. Trovarelli, J. Llorca, C. De Leitenburg, G. Dolcetti, *J. Catal.* **1998**, *178*, 299; c) D. M. Lyons, K. M. Ryan, M. A. Morris, *J. Mater. Chem.* **2002**, *12*, 1207.

[30] a) B. Smarsly, D. Grosso, T. Brezesinski, N. Pinna, C. Boissière, M. Antonietti, C. Sanchez, *Chem. Mater.* **2004**, *16*, 2948; b) D. Grosso, C. Boissière, B. Smarsly, T. Brezesinski, N. Pinna, P. A. Albouy, H. Amenitsch, M. Antonietti, C. Sanchez, *Nat. Mater.* **2004**, *3*, 787; c) M. Kuemmel, D. Grosso, C. Boissière, B. Smarsly, T. Brezesinski, P. A. Albouy, H. Amenitsch, C. Sanchez, *Angew. Chem.* **2005**, *117*, 4665; *Angew. Chem. Int. Ed.* **2005**, *44*, 4589; d) T. Brezesinski, B. Smarsly, K.-I. Iimura, D. Grosso, C. Boissière, M. Antonietti, C. Sanchez, *Small* **2005**, *1*, 889; e) T. Brezesinski, A. Fischer, K. Iimura, C. Sanchez, D. Grosso, M. Antonietti, B. Smarsly, *Adv. Funct. Mater.* **2006**, *16*, 1433; f) T. Brezesinski, D. Fattakhova Rohlfing, S. Sallard, M. Antonietti, B. Smarsly, *Small* **2006**, *2*, 1203; g) T. Brezesinski, M. Groenewolt, M. Antonietti, B. Smarsly, *Angew. Chem.* **2006**, *118*, 795; *Angew. Chem. Int. Ed.* **2006**, *45*, 781;

h) Y. Wang, T. Brezesinski, M. Antonietti, B. Smarsly, *ACS Nano* **2009**, *3*, 1373.

[31] a) T. Brezesinski, M. Antonietti, M. Groenewolt, N. Pinna, B. Smarsly, *New J. Chem.* **2005**, *29*, 237; b) T. Brezesinski, B. Smarsly, M. Groenewolt, M. Antonietti, D. Grosso, C. Boissiere, C. Sanchez, *Stud. Surf. Sci. Catal.* **2005**, *156*, 243.

[32] a) J. Roggenbuck, H. Schäfer, T. Tsoncheva, C. Minchev, J. Hanss, M. Tiemann, *Micropor. Mesopor. Mater.* **2007**, *101*, 335; b) P. Ji, J. Zhang, F. Chen, M. Anpo, *J. Phys. Chem. C* **2008**, *112*, 17809.

[33] a) A. Corma, P. Atienzar, H. García, J.-Y. Chane-Ching, *Nat. Mater.* **2004**, *3*, 394; b) A. S. Deshpande, N. Pinna, B. Smarsly, M. Antonietti, M. Niederberger, *Small* **2005**, *1*, 313.

[34] a) A. K. Sinha, K. Suzuki, *Int. J. Appl. Ceram. Technol.* **2005**, *2*, 476; b) A. K. Sinha, K. Suzuki, *J. Phys. Chem. B* **2005**, *109*, 1708.

[35] T. Brezesinski, C. Erpen, K. Iimura, B. Smarsly, *Chem. Mater.* **2005**, *17*, 1683.

[36] a) A. S. Deshpande, N. Pinna, P. Beato, M. Antonietti, M. Niederberger, *Chem. Mater.* **2004**, *16*, 2599; b) T. Baidya, A. Gupta, P. A. Deshpandey, G. Madras, M. S. Hegde, *J. Phys. Chem. C* **2009**, *113*, 4059.

[37] Y. W. Zhang, R. Si, C. S. Liao, C. H. Yan, C. X. Xiao, Y. Kou, *J. Phys. Chem. B* **2003**, *107*, 10159.

[38] a) L. J. Wu, H. J. Wiesmann, A. R. Moodenbaugh, R. F. Klie, Y. Zhu, D. O. Welch, M. Suenaga, *Phys. Rev. B* **2004**, *69*, 125415; b) S. Tsunekawa, T. Fukuda, A. Kasuya, *Surf. Sci.* **2000**, *457*, L437.

[39] S. Tsunekawa, T. Fukuda, A. Kasuya, *J. Appl. Phys.* **2000**, *87*, 1318.

[40] J. R. Mcbride, K. C. Hass, B. D. Poindexter, W. H. Weber, *J. Appl. Phys.* **1994**, *76*, 2435.

[41] a) G. A. Ozin, *Chem. Commun.* **2000**, 419; b) S. Oliver, A. Kuperman, N. Coombs, A. Lough, G. A. Ozin, *Nature* **1995**, *378*, 47.

[42] J. L. Blin, A. Leonard, Z. Y. Yuan, L. Gigot, A. Vantomme, A. K. Cheetham, B. L. Su, *Angew. Chem.* **2003**, *115*, 2978; *Angew. Chem. Int. Ed.* **2003**, *42*, 2872.

[43] B. Tian, X. Liu, B. Tu, C. Yu, J. Fan, L. Wang, S. Xie, G. D. Stucky, D. Zhao, *Nat. Mater.* **2003**, *2*, 159.

[44] L. H. Little, in, *Infrared Spectra of Adsorbed Species*, Academic Press, London **1966**, p. 193.

[45] a) A. Corma, *Chem. Rev.* **1997**, *97*, 2373; b) A. Corma, H. García, *Chem. Rev.* **2003**, *103*, 4307.

[46] T. Dogu, *Ind. Eng. Chem. Res.* **1998**, *37*, 2158.

[47] J. Yu, Y. Su, B. Cheng, *Adv. Funct. Mater.* **2007**, *17*, 1984.

[48] J. Hierso, O. Sel, A. Ringuede, C. Laberty-Robert, L. Bianchi, D. Grosso, C. Sanchez, *Chem. Mater.* **2009**, *21*, 2184.

[49] R. M. Rioux, H. Song, J. D. Hoefelmeyer, P. Yang, G. A. Somorjai, *J. Phys. Chem. B* **2005**, *109*, 2192.